13th World Conference on Earthquake Engineering
Vancouver, B.C., Canada
August 1-6, 2004
Paper No. 1170

SEISMIC PERFORMANCE OF A LAMINATED RUBBER BEARING UNDER TENSILE AXIAL LOADING

Gaku SHOJI[1], Kei SAITO[2], Toshihiro KAMEDA[3] and Taka-aki FUEKI[4]

SUMMARY

Effect of tensile axial loading on seismic performance (plastic shear deformation) of a laminated rubber bearing (LRB) was clarified. Cyclic loading tests were carried out to evaluate the relation between lateral force and lateral displacement of an LRB under seismic conditions (i.e., axial loading) and under worn conditions (i.e., 300 cycles). A strain measurement scheme based on image analysis was used to obtain the local strain fields of the LRB. Localized strain fields under tensile axial loading occurred more markedly at the corners of the free surface of the LRB than those under compressive axial loading. The seismic performance of the LRB under tensile or compressive axial loading was degraded severely after shear deformation incurred during 300 cycles.

INTRODUCTION

Isolated structural systems have been widely adopted in new construction and retrofit of buildings and bridges. Isolators play an important mechanical role in an isolated structural system to elongate the system so that the seismic force acting on the system is reduced [1],[2],[3]. Among the various types of isolators that have been developed, laminated rubber bearings (LRB) have high mechanical reliability as isolators because their shear plastic behavior becomes stable under compressive axial loading due to a dead load of a superstructure and under stress variation due to an active load [4].

Super high-rise buildings and multi-span continuous bridges have been constructed in recent years. Most of these structural systems have effective higher modes of vibration with respect to normal-size buildings and normal bridges. In the systems under the modes of vibration, extreme stress variation induced in an LRB might cause tensile axial loading [5]. Shear plastic behavior of an LRB under compressive axial loading has been clarified both theoretically and experimentally, for examples [4],[6],[7],[8], whereas that under tensile axial loading has not been sufficiently clarified.

In this study, therefore, the effect of tensile axial loading on shear plastic behavior of an LRB was clarified by conducting a series of cyclic loading tests that each yielded a hysteresis loop and local strain

[1] Assist. Prof., Inst. of Eng. Mech. and Systs., Univ. of Tsukuba, Tsukuba, Ibaraki, Japan. Email: gshoji@kz.tsukuba.ac.jp
[2] Graduate Student, Master's Prog. in Sci. and Eng., Univ. of Tsukuba, Tsukuba, Ibaraki, Japan. Email: ksaito@kz.tsukuba.ac.jp
[3] Assist. Prof., Inst. of Eng. Mech. and Systs., Univ. of Tsukuba, Tsukuba, Ibaraki, Japan. Email: kameda@kz.tsukuba.ac.jp
[4] Graduate Student, Master's Prog. in Sci. and Eng., Univ. of Tsukuba, Tsukuba, Ibaraki, Japan. Email: kfueki@kz.tsukuba.ac.jp

field of an LRB. The effect of tensile axial loading was clarified by evaluating the differences in hysteresis loops and local strain fields between an LRB under tensile axial loading and those under compressive loading.

EXPERIMENTAL SETUP AND IMAGE ANAYSIS

LRB specimens and experimental conditions

Figure 1 shows a schematic and Table 1 shows the mechanical properties of an LRB specimen. Each specimen consisted of three 8-mm-thick rubber layers and two 3-mm-thick inner steel plates. The rubber was natural rubber, whose shear modulus is 1.2MPa. Upper and lower steel plates were attached to the LRB specimen to be installed to a superstructure and a substructure. For measurement of shear deformation by image analysis, 207 points were marked on the surface of each specimen (Figure 2), because image analysis requires deformation information from a rectangular mesh generated by these marked points.

Table 1 Mechanical properties of an LRB specimen

Type of rubber (Shear modulus G)	Natural rubber (1.2MPa)
Stressed area	□250 mm×250 mm
Equivalent stressed area A_{eq}	□240 mm×240 mm
Rubber layers (Total thickness of rubber layers $\sum t_e$)	8-mm-thickness ×3 layers ($\sum t_e$ =24 mm)
Inner steel plates	3-mm-thickness×2 plates
Upper and lower steel plates	40-mm-thickness×2 plates
Total height of LRB	110 mm

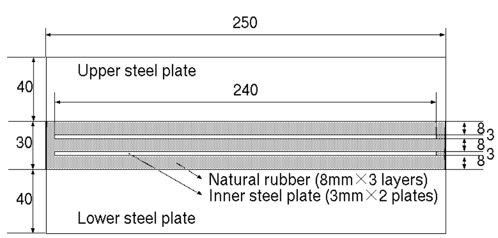

Figure 1 Schematic of an LRB specimen (dimensions in mm)

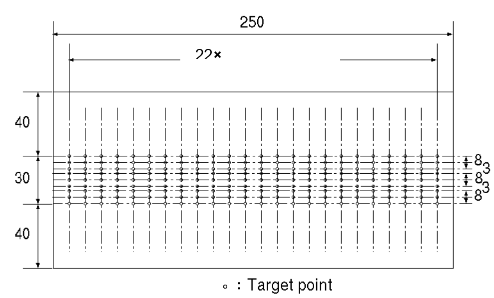

Figure 2 Marked target points (207) of LRB for measurement of shear deformation by image analysis (dimensions in mm)

Figure 3 shows the experimental setup. Each specimen was set between a girder with a horizontal actuator, a vertical actuator, and two hydraulic jacks attached, and a steel frame idealized as a substructure in a structural system. A girder was idealized as a superstructure. Keeping the vertical force driven by the vertical actuator constant, the lateral displacement applied to the LRB specimen was gradually increased by the horizontal actuator. The frequency of laterally loading on a specimen was varied from 0.005Hz to 0.01Hz.

Test cases

Table 2 lists the test cases. In this study, the global shear strain γ (in percentage) representative of the shear deformation of a specimen was defined as

$$\gamma \equiv x / \sum t_e \qquad (1)$$

where x is the shear deformation of the specimen and $\sum t_e$ is the total thickness of the rubber layers (see Table 2). Hereafter, compressive axial stress is indicated as minus (-) and tensile as plus (+).

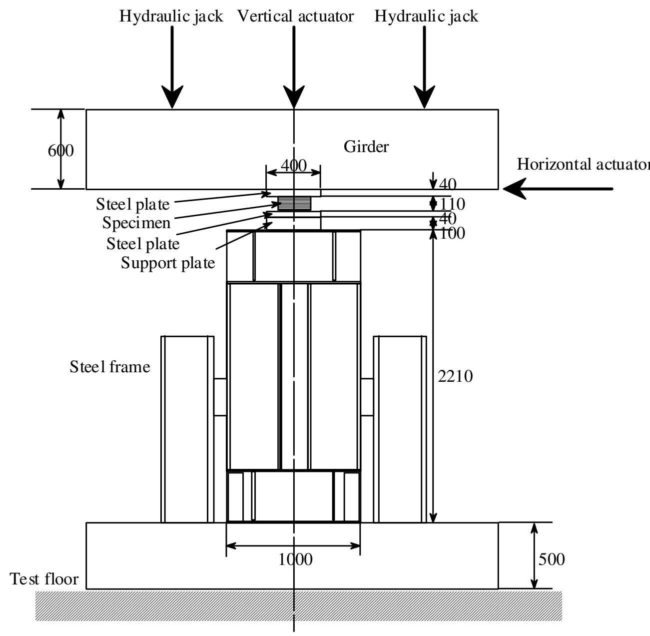

Figure 3 Experimental setup for axial loading of an LRB (dimensions in mm)

Table 2 Test cases

Test case	Axial loading + Shear deformation
Case 1	-6MPa compression + Gradually increase from γ =50% to 250%
Case 2	Zero stress + Gradually increase from γ =50% to 250%
Case 3	2MPa tension + Gradually increase from γ =50% to 250%
Case 4-1	-6MPa compression + 300 cycles of γ =90%
Case 4-2	-6MPa compression + Gradually increase from γ =50% to 250%
Case 5-1	2MPa tension + 300 cycles of γ =90%
Case 5-2	2MPa tension + Gradually increase from γ =50% to 250%

Cases 1 to 3 were used to clarify the dependence of seismic performance of the LRB on axial loading. In these three cases, either -6MPa compressive axial stress (Case 1), zero stress (Case 2), or 2MPa tensile stress (Case 3) was applied to each specimen, while γ was varied from 50% to 250%. The process of loading and unloading was repeated three times. Cases 4-1 and 5-1 were used to clarify the seismic performance of LRB under worn conditions for an LRB under compressive axial stress of -6MPa (Cases 4-1) and tensile stress of 2MPa (Case 5-1). The level of γ = 90% was assumed to be the maximum shear deformation due to the variation dependence on temperature and creep, and 300 cycles were assumed to be commutative cycles of γ = 90% during the life span of a structural system. Cases 4-2 and 5-2 were used to clarify the degradation of the seismic performance after the commutative shear deformation dependence on temperature and creep. In these two cases, the same loading procedures as Cases 1 and 3 were applied after those of Cases 4-1 and 5-1.

Image analysis

Figure 4 shows the scheme for measurement of shear deformation of an LRB by image analysis. In the first step, the deformation of an LRB during the loading was scanned by a digital video and the obtained avi-format data were transferred to bmp-format data. In the second step, the displacements and coordinates of the 207 marked target points in the x and y directions were measured. In the final step, the local strain fields ε_{xx}, ε_{yy}, and γ_{xy} at each marked point were identified based on the measured displacements and coordinates.

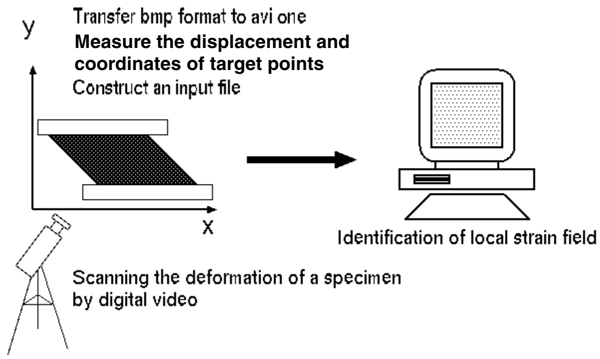

Figure 4 Scheme of image analysis for shear deformation measurement.

Values of the displacements and coordinates of the marked target points were obtained in dimensions in millimeter. A significant digit of the values has the accuracy of one digit under a decimal point since the minimum mesh size generated by the target points on the surface of each LRB and the equivalent number of pixels of the digital video were limited. Thus, values of the local strain fields ε_{xx}, ε_{yy}, and γ_{xy} have the accuracy of two digits under a decimal point as presented in the following results.

RESULTS AND DISCUSSION

Dependence of seismic performance on tensile axial loading

Figure 5 shows the hysteresis loops (lateral force versus lateral displacement) for Cases 1 to 3, and Figure 6 shows the equivalent stiffness K_{eq} and hysteretic energy dissipation per unit volume of rubber Δw as a function of γ. K_{eq} and Δw were computed as,

$$K_{eq} = \frac{P_{x_{\max}}}{x_{\max}}, \ \Delta w = \frac{1}{A_{eq} \sum t_e} \oint P(x) dx \tag{2}$$

where $x_{\max}$ is the maximum lateral displacement in the third cycle for each γ. The reason for using $x_{\max}$ in the third cycle for each γ is that we can observe the hysteresis loops in the third cycle became more stable than those in the first and second cycles in each γ. $P_{x\max}$ is the lateral force for $x_{\max}$, A_{eq} is the equivalent stressed area (see Table 2), and $P(x)$ is the lateral force for lateral displacement x. Figures 5 and 6 reveal that under tensile axial loading of 2MPa, K_{eq} was about 1.13~1.17 times larger and Δw was about 1.09~1.15 times larger compared with K_{eq} and Δw in another cases. It indicates that the effect of tensile axial loading on the hysteresis loop appeared when γ exceeded about 150%.

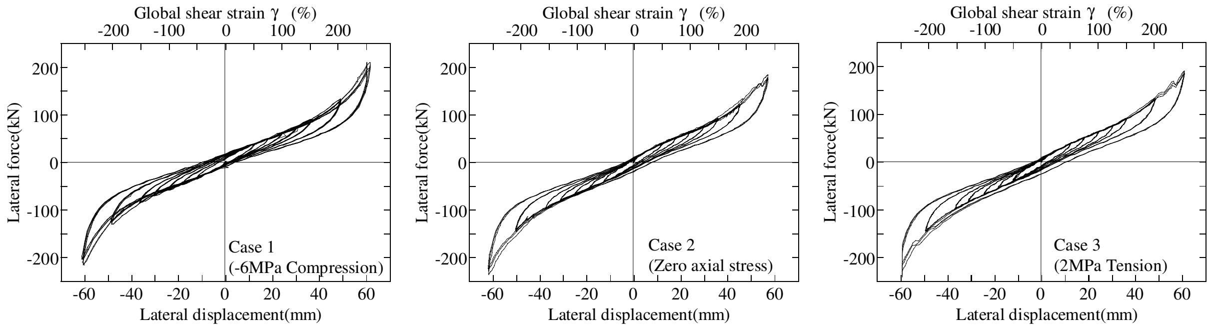

Figure 5 Lateral force versus lateral displacement for Cases 1~3

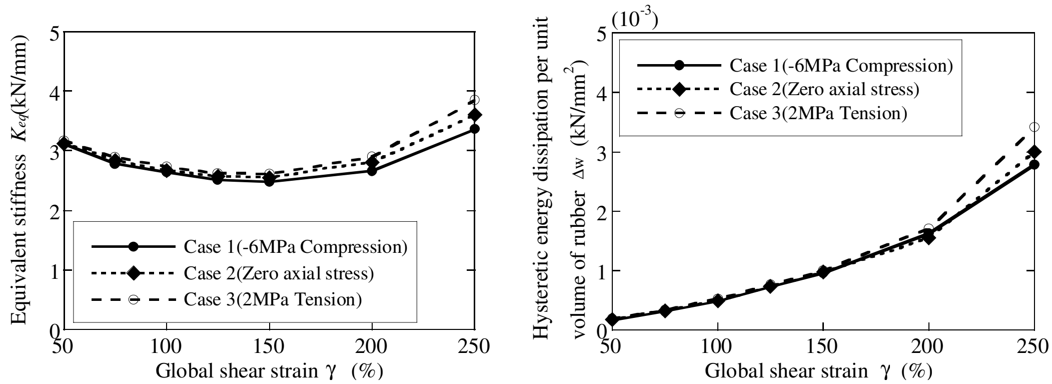

Figure 6 Equivalent stiffness K_{eq} and hysteretic energy dissipation per unit volume of rubber Δw for Cases 1~3

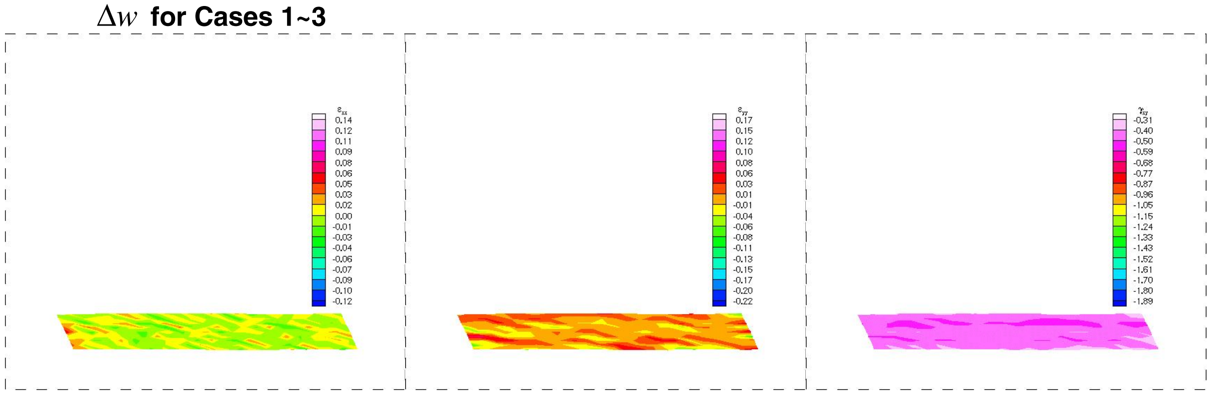

i) ε_{xx} ii) ε_{yy} iii) γ_{xy}

(a) Global shear strain γ =75%

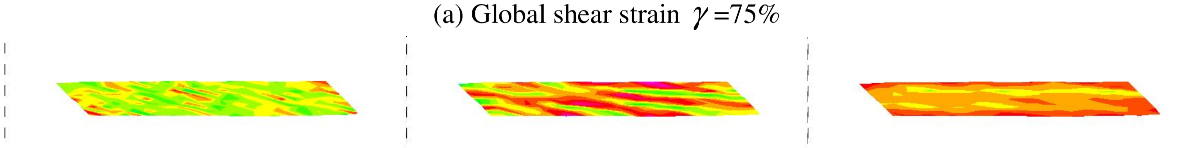

i) ε_{xx} ii) ε_{yy} iii) γ_{xy}

(b) Global shear strain γ =150%

Figure 7 Local strain fields for Case 1

Figures 7 and 8 show the local strain fields ε_{xx}, ε_{yy}, and γ_{xy} when γ = 75% and 150% obtained from image analysis for Cases 1 and 3 to compare the difference of local strain fields between compressive and tensile cases. Note that the legends in Figure 7a apply also to all other figures of the local strain fields, namely, Figures 8, 12 and 13.Under compressive axial loading (Figure 7b), a large area of the LRB showed ε_{xx} between -0.03~0.02 and ε_{yy} between 0.10~0.12. Under tensile axial loading (Figure 8b), a large area of the LRB showed ε_{xx} of 0.02~0.06 and γ_{xy} of -1.15~-1.05, while the corners along free surfaces showed a large ε_{xx} of 0.06. Although the hysteresis loop weakly depended on axial loading (see Figures 5 and 6), the local strains and their spatial distribution strongly depended on axial loading (see Figures 7 and 8).

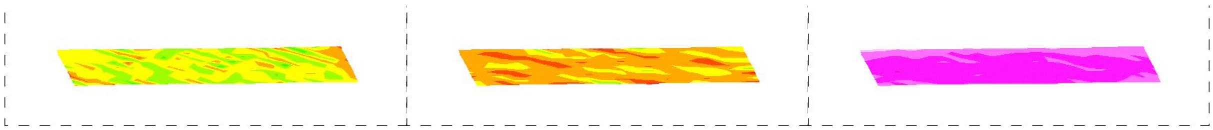

i) ε_{xx} ii) ε_{yy} iii) γ_{xy}

(a) Global shear strain γ =75%

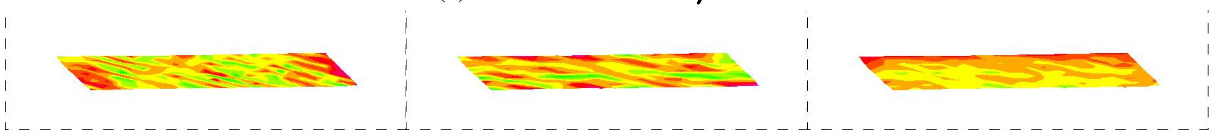

i) ε_{xx} ii) ε_{yy} iii) γ_{xy}

(b) Global shear strain γ =150%

Figure 8 Local strain fields for Case 3

Dependence of seismic performance on worn conditions

Figure 9 shows the hysteresis loops for Cases 4-1 and 5-1. In these hysteresis loops, the reduction ratio η in terms of the maximum lateral force $P\left(x_i^{\max}\right)$ was defined as,

$$\eta = P\left(x_i^{\max}\right) / P\left(x_1^{\max}\right) \tag{3}$$

where $P\left(x_1^{\max}\right)$ or $P\left(x_i^{\max}\right)$ is the lateral force corresponding to the maximum lateral displacement $x_1^{\max}$ or $x_i^{\max}$ in the 1st or i th cycle. Figure 10 shows η calculated using Equation (3). Figures 9 and 10 reveal that after 300 cycles, η for an LRB under either compressive or tensile axial loading reached as high as 0.8~0.9. Such a high η indicates that the plastic shear deformation under either compressive or tensile axial loading was severely degraded after the shear deformation incurred during 300 cycles due to thermal variation and creep.

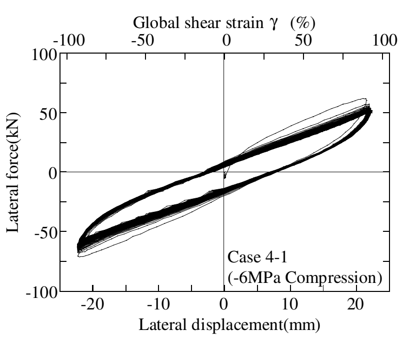

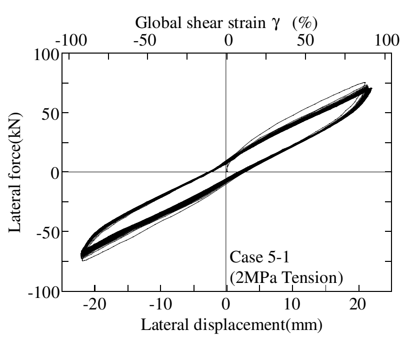

Figure 9 Lateral force versus lateral displacement for Cases 4-1 and 5-1

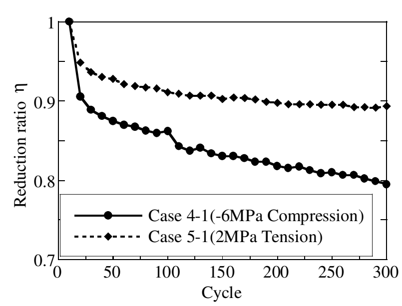

Figure 10 Reduction ratio η for Cases 4-1 and 5-1

Figure 11 shows K_{eq} and Δw as a function of γ for Cases 4-2 and 5-2. Independent of γ, K_{eq} was about 10~20% larger and Δw was about 10~20% smaller under tensile axial loading of 2MPa than under compressive loading of -6MPa. It suggests that the hysteresis loop under tensile axial loading became narrower. Comparing Figure 11 with Figure 6 reveals that after 300 cycles the effect of axial loading on the seismic performance of an LRB was more pronounced.

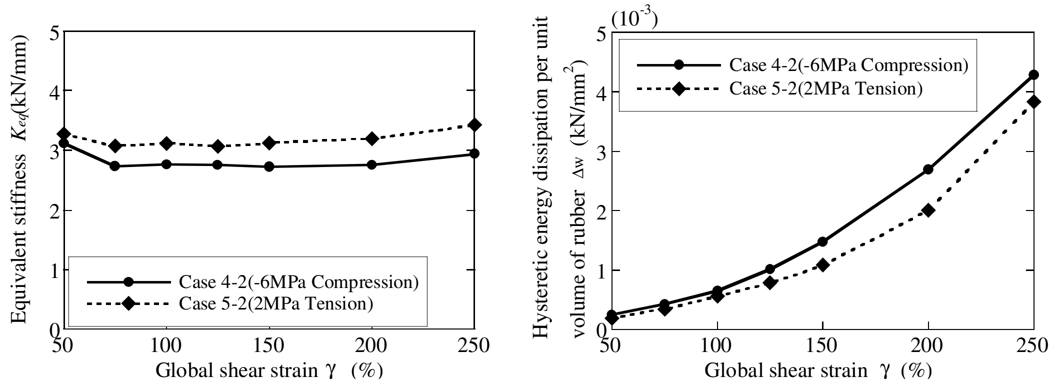

Figure 11 Equivalent stiffness K_{eq} and hysteretic energy dissipation per unit volume of rubber Δw for Cases 4-2 and 5-2

Figures 12 and 13 show the local strain fields for Cases 4-2 and 5-2, respectively. After 300 cycles, the local strain fields ε_{xx}, ε_{yy}, γ_{xy} were higher and the region where dominant strain fields occurred was broader under compressive axial loading than under tensile loading (see Figures 7, 8, 12, and 13). Under compressive axial loading, the degradation of rubber layers during 300 cycles might result in further reduction in seismic performance of an LRB. The LRB under compressive axial loading had large localized shear strain fields at the rubber layers underneath and on the inner steel plates (see Figure 12b), whereas the LRB under tensile axial loading had such large fields at the rubber layers around the upper and lower steel plates (see Figure 13b).

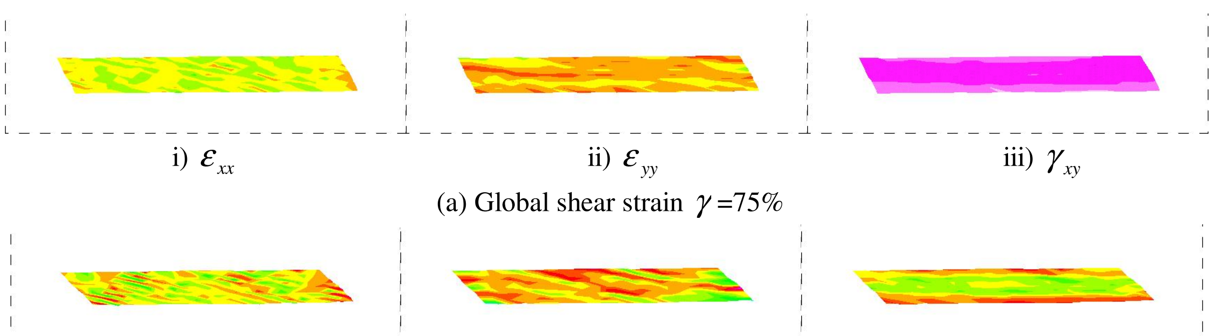

i) ε_{xx} ii) ε_{yy} iii) γ_{xy}

(a) Global shear strain γ =75%

i) ε_{xx} ii) ε_{yy} iii) γ_{xy}

(b) Global shear strain γ =150%

Figure 12 Local strain fields for Case 4-2

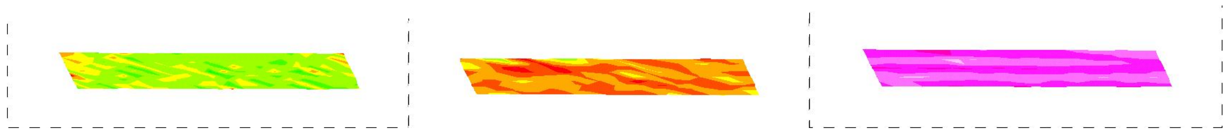

i) ε_{xx} ii) ε_{yy} iii) γ_{xy}

(a) Global shear strain γ =75%

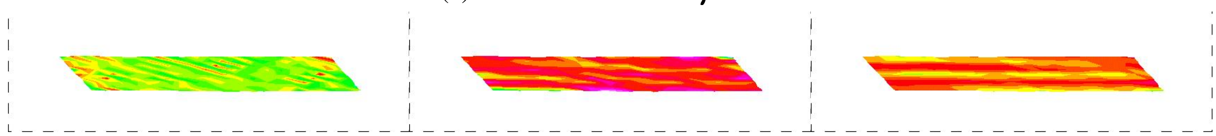

i) ε_{xx} ii) ε_{yy} iii) γ_{xy}

(b) Global shear strain γ =150%

Figure 13 Local strain fields for Case 5-2

CONCLUSIONS

A series of cyclic loading tests under seismic conditions (i.e., axial loading) and worn conditions (i.e., 300 cycles) were conducted to clarify the effect of tensile axial loading on plastic shear deformation of a laminated rubber bearing (LRB). Each LRB specimen was subjected to three cycles of lateral deformation that was gradually varied from a global shear strain γ of 50% to 250%. Hysteretic loops between lateral force and lateral displacement were evaluated to compare hysteretic energy dissipation and equivalent stiffness between an LRB under tensile axial loading and under compressive loading. The local strain fields ε_{xx}, ε_{yy}, γ_{xy} of the LRB were measured by using image analysis. The following four key results were revealed.

1) Under tensile axial loading, the equivalent stiffness K_{eq} was about 1.13~1.17 times larger and hysteretic energy dissipation per unit volume of rubber Δw was about 1.09~1.15 times larger compared with K_{eq} and Δw under compressive and zero axial loading. It indicates that although the effect of tensile axial loading on the hysteresis loop appeared when γ exceeded about 150%, the hysteresis loop weakly depended on axial loading.

2) Although the hysteresis loop weakly depended on axial loading, the local strains ε_{xx}, ε_{yy}, γ_{xy} and their spatial distribution strongly depended on axial loading. Localized strain fields occurred at the corners of rubber layers of an LRB when γ exceeded about 150%. This trend became more notable for an LRB under tensile axial loading than under compressive axial loading.

3) After 300 cycles, the local strain fields were higher and the region where dominant strain fields occurred was broader under compressive axial loading than under tensile loading. Under compressive axial loading, the degradation of rubber layers during 300 cycles might result in further reduction in seismic performance of an LRB.

4) After 300 cycles, for an LRB under compressive axial loading, large localized shear strain fields occurred at the rubber layers underneath and on the inner steel plates. In contrast, for an LRB under tensile axial loading, such large strain fields occurred at the rubber layers around the upper and lower steel plates.

ACKNOWLEDGEMENTS

The authors appreciate the valuable support and assistance from the personnel at the companies belonging to the Institute of Rubber Bearing, Japan, and appreciate the assistance from Mr. A. Kojima at the Institute of Engineering Mechanics and Systems, University of Tsukuba, in the cyclic loading tests.

REFERENCES

1. Buckle IG. and Mayes RL. "Seismic isolation: history, application and performance – a world view." Earthquake Spectra, 1990; 6(2): 161-201.
2. Kawashima K., Hasegawa K. and Nagashima H. "A perspective of Menshin design of highway bridges in Japan." Proceeding of First US-Japan Workshop on Earthquake Protective Systems for Bridges, National Center for Earthquake Engineering Research, State University of New York, Buffalo, USA, 1992; 92(4): 3-25.
3. Skinner I., Robinson WH. and McVerry GH. "An introduction to seismic isolation." USA; John Wiley & Sons, 1993.
4. Kelly JM. "Earthquake-Resistant Design with Rubber." 2nd Edition, Springer, 1997.
5. Takahashi Y., Iemura H., Ogawa K., Nakajima K. and Tamaki T. "Effects of Vertical Ground Motion to Seismically Isolated Friction Bearing with Hybrid Loading Tests." Proceeding of 7th East Asia-Pacific Conference on Structural Engineering and Construction, Kochi, Japan, 1999: 824-829.
6. Gent AN. and Meinecke EA. "Compression, bending and shear of bonded rubber blocks." Polymer Engineering and Science, 1970; 10(1): 48-53.
7. Mori A., Carr AJ. , Cooke N. and Moss PJ. "Compression Behaviour of Bridge Bearings used for Seismic Isolation." Engineering Structures, 1996; 18(5): 351-362.
8. Hamzeh ON., Tassoulas JL. and Becker EB. "Behavior of elastomeric bridge bearings: computational results." Journal of Bridge Engineering, ASCE, 1998; 3(3): 140-146.